Kinetic features of phase separation under alloy ordering

V. Yu. Dobretsov and V. G. Vaks
Russian Research Centre ''Kurchatov Institute,'' Moscow 123182, Russia

G. Martin
Centre d'Etudes de Saclay, Section de Recherches de Métallurgie Physique, 91191 Gif-sur-Yvette CEDEX, France
(Received 26 February 1996; revised manuscript received 23 April 1996)

The microscopic mean-field kinetic equation (MFKE) proposed earlier is used to investigate the kinetics of alloy decomposition in the presence of alloy ordering. A strong interaction between order and concentration fields results in a number of peculiarities in microstructural evolution. The kinetics of spinodal decomposition in ordered alloys has a number of distinct features as compared to disordered alloys; in particular, the amplification factor of the unstable composition fluctuations increases as the distance to the ordering spinodal rather than as the square of the distance to the usual spinodal for disordered alloys. Microstructural evolution is studied using computer simulations based on the MFKE. A great variability of transient microstructures as well as a high sensitivity of the type of evolution to alloy composition, annealing temperature and thermal history has been found. We describe a peculiar kinetic phenomenon which occurs in the regime of spinodal decomposition with ordering: Antiphase boundaries ''replicate,'' generating approximately periodic patterns. We discuss available experimental indications for this replication of antiphase boundaries.
[S0163-1829(96)07829-0]

I. INTRODUCTION

Ordering of alloys is often accompanied by phase separation. Such is the case, for example, when an initially homogeneous alloy is quenched into the region of two-phase equilibrium between the ordered and disordered phases in the concentration-temperature (c-T) phase diagram. Kinetic features of such transformations received recently much attention: see, e.g., Refs. 1–5. The character of the microstructural evolution is determined by the relative position in the phase diagram of the initial point c,T relative to the ordering spinodal $T_{os}(c)$, i.e., the instability limit of the disordered phase with respect to ordering. When $T>T_{os}(c)$ [area (c) in Fig. 1], decomposition into the ordered and disordered phases is realized via the usual nucleation and growth mechanism, with no qualitative difference with other first-order phase transitions, e.g., the decomposition of an alloy into two disordered phases. However, at $T<T_{os}(c)$ [area (d) or (e) in Fig. 1], the kinetic evolution becomes complex and peculiar, due to the presence of a number of simultaneous kinetic processes with different relaxation times: ordering, formation, and growth of antiphase domains, precipitation of ordered and disordered phases, etc.

Kinetic features of such phase transformations have been qualitatively discussed by Allen and Cahn[1] (AC) in their study of the Fe-Al alloy, the phase diagram of which is similar to that presented in Fig. 1 in a certain range of concentrations and temperatures. AC noted that the transformation kinetics here should have a ''two-step'' character. First, for a relatively short time $t\sim\tau$, where τ is the effective time for one intersite atomic exchange, the degree of order η achieves its equilibrium value with the local concentration c: $\eta=\eta_0(c,T)$, where the function $\eta_0(c,T)$ corresponds to the equilibrium homogeneous alloy. Further changes of the alloy state correspond to variations of the local concentration c. They are realized via diffusion of atoms for considerable distances, which needs many intersite jumps for each atom and thus much longer times $t_d\gg\tau$. Therefore, if we have some expression for the Landau-type homogeneous free energy $F(c,\eta,T)$, it is natural to define the adiabatic (or ''conditional''[1]) free energy $F_a(c,T)=F[c,\eta_0(c,T),T]$ that can be used to describe these slowly varying ''partially equilibrated'' or ''macrononequilibrium'' states (see Ref. 6, Sec. 4) being equilibrated only over the ''rapid'' variable η. Using these considerations, AC defined together with F_a the conditional spinodal line $T_{cs}(c)$, defined in the c,T plane by the equation $(\partial^2F_a/\partial c^2)_T=0$, similarly to the definition of usual spinodals for disordered alloys.[7] Then stan-

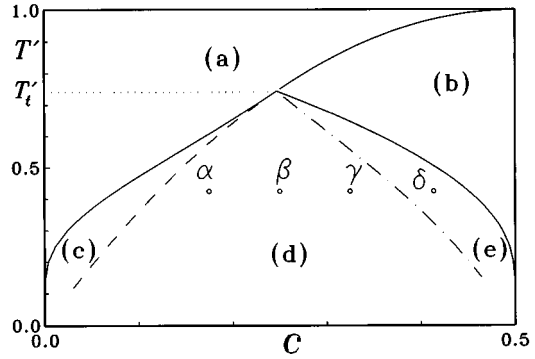

FIG. 1. Equilibrium phase diagram $(T',c)=(T/T_c,c)$ for the alloy model used. Solid lines, boundaries of the disordered (a) and homogeneous ordered (b) fields; areas (c), (d), and (e) correspond to the two-phase region. Dashed line, ordering spinodal $T_{os}(c)$; dot-dashed line, conditional spinodal $T_{cs}(c)$; both lines cross at the tricritical point T_t,c_t. Points α, β, γ, and δ show the alloy compositions and temperatures chosen for the computer simulations described in Sec. III.

 © 1996 The American Physical Society

dard arguments show that at temperatures below $T_{cs}(c)$ the homogeneous alloy is unstable with respect to long-wave concentration fluctuations: Spinodal decomposition (SD) should occur. Therefore, when the initial point c,T lies below both $T_{os}(c)$ and $T_{cs}(c)$ [area (d) in Fig. 1], the alloy can decompose via SD, while at $T_{cs}(c)<T$ [area (e) in Fig. 1] the decomposition is realized via nucleation and growth.

AC also noted that the presence of antiphase boundaries (APB's) in the initial state (once the first-step local ordering has been accomplished) should have a significant effect on the decomposition kinetics. This effect is related to segregation at APB's of the major component in nonstoichiometric alloys.[8,9] Such a segregation, combined with the depletion of the order parameter within the APB, makes the APB a possible embryo for the formation of the disordered phase. Therefore, one more important parameter determining the transformation kinetics is the density of APB's or the characteristic size l of the ordered domains in the initial state. The type of microstructural evolution under SD is determined by the relation between l and the wavelength λ_c of the fastest growing concentration waves, to be called the ''critical'' concentration waves. The value of λ_c determines the characteristic period of the microstructure at the first stages of SD.[7,10] When $l \gg \lambda_c$, the presence of APB's should have little effect on SD, while for $l \lesssim \lambda_c$, the precipitation of the disordered phase starts mainly on APB's. Similarly, in area (e) of Fig. 1, APB's can serve as embryos for nucleation of the disordered phase.

The qualitative considerations of AC have been supported by a number of experiments; see, e.g., Refs. 1,2, and 4. In particular, transient microstructures typical of SD have been observed in Fe-Al alloys after quenching to c,T values supposed to correspond to area (d) in Fig. 1.[1,2] At the same time, a minor variation of c and T, from $c_1=c_1^{Al}=0.247$, $T_1=841$ K to $c_2=0.249$, $T_2=843$ K, drastically changed the type of microstructural evolution, converting it into that characteristic of nucleation growth.[2] This can be naturally explained if one supposes that the transition from c_1,T_1 to c_2,T_2 corresponds to the transition from area (d) to (e) in Fig. 1.

In their work[1] AC discussed only the most general features of phase transformations, using mainly thermodynamic arguments. Thus they did not consider details of the kinetic processes. In particular, they did not present the linear stability analysis for the ordered homogeneous alloy in the unstable region, similar to that given by Cahn[7] for the disordered phase. Such an analysis would provide, in particular, explicit expressions for the main kinetic characteristics of the first stage of SD, the wavelength $\lambda_c(c,T)$, and the amplification factor (increment) $p_c(c,T)$ of the critical concentration waves.[7,10] AC discussed neither the variation of transient morphologies with concentration c and temperature T within each area of Fig. 1 nor the evolution of isolated APB's under SD, nor other microscopic details of the evolution. To treat these problems, elaboration of microscopic kinetic models is evidently needed.

Later some of the considerations of AC were illustrated by Chen and Khachaturyan[3–5] (CK) with computer simulations based on a simplified kinetic equation. The latter corresponds to some arbitrary extrapolation of the phenomenological Onsager equation (see Ref. 6, Sec. 120), describing the relaxation of weakly nonequilibrium systems, to the essentially nonequilibrium region. CK discussed mainly the quench $a \rightarrow d$ in Fig. 1 at $l \lesssim \lambda_c$, illustrating the above-mentioned two-step character of the evolution and precipitation of the disordered phase along APB's at first stages of SD. CK also simulated the $a \rightarrow e$ type quench,[3] but it seems that the decomposition stage has not been achieved in this simulation (see below).

Recently we proposed a mean-field kinetic equation (MFKE) to treat the configurational kinetics of alloys at an arbitrary degree of nonequilibrium.[9–11] As in other statistical problems, the mean-field approach (MFA) correctly describes the main qualitative features of phenomena, while for systems with long-range interactions its results can be true even quantitatively.[12,13] As was discussed in Ref. 10, the above-mentioned equation of CK (Refs. 3–5) corresponds to a partial linearization of the MFKE, and will therefore be referred to as the ''partially linearized kinetic equation'' (PLKE). Unlike the PLKE, the MFKE takes into account the dependence of microscopic kinetic coefficients on local values of η and c. Thus the MFKE can be used to study not only general trends of structural evolution, but also strictly kinetic problems, such as the concentration, temperature, and time dependence of kinetic characteristics. This was illustrated in Ref. 9 with a microscopic investigation of the APB motion. Here we apply the MFKE to study kinetic features of alloy decomposition under ordering.

In Sec. II we present the above-mentioned stability analysis for the ordered alloy quenched into area (d) of Fig. 1, to illustrate and specify the general considerations of AC (Ref. 1) about the features of ''conditional'' SD. We found a number of peculiarities in the kinetics of these SD, due to the presence of a strong coupling between local fluctuations of c and η. In particular, the dependences of increments p of the concentration waves for this SD, on c, T and the wave number $\mathbf{k}$, differ noticeably from those for conventional SD in disordered alloys,[7] particularly when c,T values are close to the ordering spinodal $T_{os}(c)$.

In Sec. III we investigate the features of microstructural evolution after various type of quenches: (a)$\rightarrow$(d), (b)$\rightarrow$(d), and (a)$\rightarrow$(e) in Fig. 1. We use simulations based on the MFKE for the same two-dimensional alloy model as that in Refs. 3–5. Our results illustrate a significant sensitivity of the type of evolution to the quenching conditions, in particular, to the position of the initial c,T point in the phase diagram. We also discuss a number of features of evolution not mentioned earlier: the respective importance of the ''coagulation''[10] and ''evaporation-condensation''[14] mechanisms of precipitation at different stages of coarsening, growth of a disordered single-connected precipitate from the initial APB-shaped embryo, etc. To estimate the scale and character of errors brought about by using the PLKE instead of the full MFKE, we also compare our results with those of Refs. 3–5 and conclude that the errors can be significant.

In Sec. IV we discuss an unusual type of microstructural evolution under SD that can arise near an isolated APB. It may occur, for example, when the alloy first annealed in area (b) is quenched into area (d) in Fig. 1. We show that certain approximately periodic structures replicating the initial APB shape can be formed here at intermediate stages of evolution. We also discuss possible evidence of this peculiar self-

organization phenomenon in available experimental data.[1,2]

In Sec. V we discuss the accuracy of our MFKE in describing phase transformation kinetics. To this end we apply this equation to the problem of transient ordered states under phase separation into disordered phases, which has been studied earlier by CK using the PLKE,[15] and also by Reinhardt and Turchi using Monte Carlo simulation.[16] Our MFKE results show good qualitative agreement with those of Ref. 16, which seems to support the applicability of the MFKE to problems treated in the present work. Our main conclusions are summarized in Sec. VI.

II. SPINODAL DECOMPOSITION OF THE ORDERED ALLOY

In this section we investigate the time evolution of small fluctuations in the local concentration and order parameter values for the ordered homogeneous alloy. This analysis generalizes that given by Cahn[7] in his discussion of SD in disordered alloys (SDDA). The initial stage of SD described by linear equations in this section will be called for brevity the ''Cahn stage.''

We consider a binary A-B alloy and use the ''thermally activated direct exchange'' model[12,17] to describe intersite jumps of atoms. The time evolution of the mean occupation number c_i of lattice site i by an atom A is described by the MFKE as[10]

$$\frac{dc_i}{dt}=\sum_s \gamma_{is}[c_i' c_s \exp(\varphi_s^A+\varphi_i^B)-c_s' c_i \exp(\varphi_i^A+\varphi_s^B)]. \tag{1}$$

Here $\gamma_{is}=\gamma_{si}$ is the c_i-independent part of the jump probability, $c_i'=1-c_i$, $\varphi_i^p=\beta(v^p c)_i$, $\beta=1/T$ is the reciprocal temperature, $(v^p c)_i=\Sigma_j v_{ij}^p c_j$ is the MF potential acting on a p species located at site i, and v_{ij}^A and v_{ij}^B are related to the configurational potential $v=V^{AA}+V^{BB}-2V^{AB}$ and the ''asymmetric'' one $u=V^{AA}-V^{BB}$ as $v^A=1/2\,(u+v)$, $v^B=1/2\,(u-v)$. Both the jump probability γ_{ij} and the interaction potentials v_{ij}, u_{ij} are supposed to depend only on the intersite distance $\mathbf{r}_{ij}=\mathbf{r}_i-\mathbf{r}_j$: $\gamma_{ij}=\gamma(\mathbf{r}_{ij})$, $v_{ij}=v(\mathbf{r}_{ij})$, and $u_{ij}=u(\mathbf{r}_{ij})$. The potentials u and v are supposed to have a finite range of interaction: Specific effects of long-ranged elastic interactions[4,5] are not discussed in this work.

First, we consider the case of a disordered alloy, to compare the MFKE results with those of the phenomenological approach.[7] For such an alloy the initial mean occupation $\langle c_i\rangle=c$ is the same for all sites i. To study the time evolution of small fluctuations $\delta c_i=c_i-c$, we linearize the MFKE (1) in $\delta c_i=\delta c(\mathbf{r}_i)$ and proceed to their Fourier components $\delta c_{\mathbf{k}}=\Sigma_{\mathbf{r}}\delta c(\mathbf{r})\exp(i\mathbf{kr})$. Writing $\delta c_{\mathbf{k}}=\delta c_{\mathbf{k}}(t)$ as $\delta c_{\mathbf{k}}^0\exp(pt)$, we obtain after standard manipulations

$$p=p(\mathbf{k})=m\gamma_{0\mathbf{k}}(-\mathbf{z}-\varphi_{\mathbf{k}}), \tag{2a}$$

$$m=cc'\exp(\beta u_0 c). \tag{2b}$$

Here and below $z=1/cc'$, $c'=1-c$, $\gamma_{0\mathbf{k}}=\gamma_0-\gamma_{\mathbf{k}}$, and $\varphi_{\mathbf{k}}=\beta v_{\mathbf{k}}$. The factor m in Eqs. (2) determines the concentration dependence of the mobility M,[17] while $\gamma_{\mathbf{k}}$, $\gamma_0=\gamma_{\mathbf{k}=0}$, $v_{\mathbf{k}}$, and $u_0=u_{\mathbf{k}=0}$ are the Fourier components of the functions $\gamma(\mathbf{r})$, $v(\mathbf{r})$, and $u(\mathbf{r})$:

$$\gamma_{\mathbf{k}}=\sum_{\mathbf{r}}\gamma(\mathbf{r})\exp(i\mathbf{k}\cdot\mathbf{r}),\quad v_{\mathbf{k}}=\sum_{\mathbf{r}}v(\mathbf{r})\exp(i\mathbf{k}\cdot\mathbf{r}),$$

$$u_{\mathbf{k}}=\sum_{\mathbf{r}}u(\mathbf{r})\exp(i\mathbf{k}\cdot\mathbf{r}).$$

The reduced free energy $f=\beta F$ (per site) in the MFA used here has the form (see, e.g., Ref. 10)

$$f=c\ln c+c'\ln c'+\tfrac{1}{2}\varphi_0 c^2. \tag{3}$$

The spinodal curve $T_s(c)$ is defined by the equation $\partial^2 f/\partial c^2\equiv f_{cc}=0$; below T_s, f_{cc} is negative. In our case $f_{cc}=z+\varphi_0$; thus Eq. (2a) can be written as

$$p(\mathbf{k})=m\gamma_{0\mathbf{k}}(-\mathbf{f}_{cc}-\varphi_{\mathbf{k}0}), \tag{4}$$

where $\varphi_{\mathbf{k}0}=\varphi_{\mathbf{k}}-\varphi_0$. As the interaction $v_{\mathbf{k}}$ is most attractive (negative) at $k=0$, the difference $\varphi_{\mathbf{k}0}$ in (4) is positive; such is also the case for the factor $\gamma_{0\mathbf{k}}$ which is the sum of positive terms $\gamma(\mathbf{r})(1-\cos\mathbf{kr})$. In the case of small k in the cubic lattice (treated in Ref. 7) Eq. (4) takes the form

$$p(\mathbf{k})=M'k^2(-f_{cc}-\Lambda k^2), \tag{5}$$

where $M'k^2$ and Λk^2 mean expansions of the difference $m\gamma_{0\mathbf{k}}$ and, respectively, $\varphi_{\mathbf{k}0}$ at small k. Equation (5) for $p(\mathbf{k})$ coincides with that of Cahn[7] and provides the microscopic expression for his phenomenological parameters M, 2κ and $M'T$, ΛT, respectively, in our notation. According to this equation, the wave number $k_c=2\pi/\lambda_c$ and the increment $p_c=p_{\max}$ for critical concentration waves are given by

$$k_c=(-f_{cc}/2\Lambda)^{1/2},\quad p_c=M'f_{cc}^2/4\Lambda. \tag{6}$$

The full equation (4) extends the results of Ref. 7 to arbitrary wave numbers $\mathbf{k}$ in the Brillouin zone, and thus to not necessarily small f_{cc} and large λ_c values at SD.

For the ordered phase with ν different sublattices α, the site numbers i,j in Eq. (1) are replaced with a pair of indices: $i\to m\alpha$, $v_{ij}\to v_{mn}^{\alpha\beta}$, where m or n now number different ν atomic cells. As in Refs. 1–5,9, for simplicity we consider only structures made of two equivalent sublattices 1 and 2, such as the $B2$ or $L1_0$ ordered phases. Then it is convenient to define the local ''cell'' values of the concentration and the order parameter, c_m and η_m, by the relations $c_{1m}=c_m+\eta_m$, $c_{2m}=c_m-\eta_m$. Under perfect ordering, the quantities $c_m=c(\mathbf{R}_m)$ and $\eta_m=\eta(\mathbf{R}_m)$ are periodic in the cell coordinate $\mathbf{R}_m$ with periods of the ordered structure. These periods exceed those of the original, disordered lattice; for example, periods of the cubic $B2$ phase exceed those of the underlying bcc lattice.

In the stability analysis we write $c(\mathbf{R})$ or $\eta(\mathbf{R})$ as the sum of the lattice average, $c=\langle c(\mathbf{R})\rangle$ or $\eta=\langle\eta(\mathbf{R})\rangle$, and of small fluctuations that we write as Fourier series:

$$c(\mathbf{R}) = c + \sum_{\mathbf{k}} \delta c_{\mathbf{k}} \exp(-i\mathbf{k}\mathbf{R}),$$

$$\eta(\mathbf{R}) = \eta + \sum_{\mathbf{k}} \delta \eta_{\mathbf{k}} \exp(-i\mathbf{k}\mathbf{R}). \tag{7}$$

Proceeding in Eq. (1) from variables c_{1m} and c_{2m} to c_m and η_m, using Eqs. (7), and expanding the resulting kinetic equations in $\delta c_{\mathbf{k}}$ and $\delta \eta_{\mathbf{k}}$, we obtain the zero-order equation for the long-range order parameter $\eta(t)$ and the set of linear equations for $\delta c_{\mathbf{k}}$ and $\delta \eta_{\mathbf{k}}$ that describe fluctuation waves with $\mathbf{k} \neq 0$.

To write these equations, it is convenient to simplify the notation of Fourier components of the functions $\gamma^{\alpha\beta}(\mathbf{R})$, $u^{\alpha\beta}(\mathbf{R})$, and $v^{\alpha\beta}(\mathbf{R})$. To this end, instead of the intersublattice potentials $u^{\alpha\beta}(\mathbf{R})$ and $v^{\alpha\beta}(\mathbf{R})$, we define their linear combinations u, $\tilde{u}$, v, and $\tilde{v}$:

$$u = u^{11} + u^{12}, \quad \tilde{u} = u^{11} - u^{12},$$

$$v = v^{11} + v^{12},$$

$$\tilde{v} = v^{11} - v^{12}. \tag{8}$$

Fourier components of potentials (8) and of functions $\gamma^{\alpha\beta}(\mathbf{R})$ are sums over cell coordinates $\mathbf{R}$ in the ordered phase. We rewrite these components as sums over true intersite distances, i.e., over lattice vectors $\mathbf{r}$ in the disordered phase. Let us define the ordered phase superstructure vector $\mathbf{k}_s$ by the relations $\exp(i\mathbf{k}_s\mathbf{r}) = 1$ when the lattice vector $\mathbf{r}$ connects sites of the same sublattice, 1 and 1 or 2 and 2, and $\exp(i\mathbf{k}_s\mathbf{r}) = -1$ when $\mathbf{r}$ connects different sublattices, 1 and 2. For example, for the $B2$ phase, $\mathbf{k}_s = (1,1,1)2\pi/a$ where a is the bcc lattice constant. Then the Fourier components $\gamma_{\mathbf{k}}^{\alpha\beta}$, $u_{\mathbf{k}}$, $v_{\mathbf{k}}$, $\tilde{u}_{\mathbf{k}}$, and $\tilde{v}_{\mathbf{k}}$ can be written in a ''covariant'' form:

$$\gamma_{\mathbf{k}}^{11} = \gamma_{\mathbf{k}}^{22} = \frac{1}{2}\sum_{\mathbf{r}} \gamma(\mathbf{r})[1 + \exp(i\mathbf{k}_s\mathbf{r})]\exp(i\mathbf{k}\mathbf{r}),$$

$$\gamma_{\mathbf{k}}^{12} = \gamma_{\mathbf{k}}^{21} = \frac{1}{2}\sum_{\mathbf{r}} \gamma(\mathbf{r})[1 - \exp(i\mathbf{k}_s\mathbf{r})]\exp(i\mathbf{k}\mathbf{r}),$$

$$\{u_{\mathbf{k}}, v_{\mathbf{k}}\} = \sum_{\mathbf{r}} \{u(\mathbf{r}), v(\mathbf{r})\}\exp(i\mathbf{k}\mathbf{r}),$$

$$\{\tilde{u}_{\mathbf{k}}, \tilde{v}_{\mathbf{k}}\} = \sum_{\mathbf{r}} \{u(\mathbf{r}), v(\mathbf{r})\}\exp(i\mathbf{k}_s\mathbf{r} + i\mathbf{k}\mathbf{r}).$$

Using this notation we can write the above-mentioned zero-order equation for $\eta(t)$:

$$\frac{d\eta}{dt} = -\gamma_0^{12} e^{\beta u_0 c}(c_1 c_2' e^{\tilde{\varphi}_0 \eta} - c_1' c_2 e^{-\tilde{\varphi}_0 \eta}), \tag{9}$$

where $c_{1,2} = c \pm \eta$ and $c_{1,2}' = c' \mp \eta$, while γ_0^{12}, u_0, and $\tilde{\varphi}0(13)$ are $\mathbf{k} = 0$ values of Fourier components $\gamma_{\mathbf{k}}^{12}$, $u_{\mathbf{k}}$, and $\tilde{\varphi}_{\mathbf{k}} = \beta\tilde{v}_{\mathbf{k}}$. Equation (9) describes the relaxation of the long-range order parameter η.

The MFA expression for the reduced free energy $f = \beta F$ per site, generalizing Eq. (3) to the ordered phase, has the form[10]

$$f = \frac{1}{2}(c_1 \ln c_1 + c_2 \ln c_2 + c_1' \ln c_1' + c_2' \ln c_2') + \frac{1}{2}\varphi_0 c^2 + \frac{1}{2}\tilde{\varphi}_0 \eta^2, \tag{10}$$

where φ_0 is the same as in Eq. (3). Using Eq. (10) we can rewrite Eq. (9) as

$$\frac{d\eta}{dt} = -\gamma_0^{12} \exp(\beta u_0 c)(c_1 c_1' c_2 c_2')^{1/2} 2\sinh(\partial f/\partial \eta), \tag{11}$$

which is a particular case of the general MFKE (Ref. 18) for the uniform ordering relaxation. Equations (9)–(11) show that the stationary state $d\eta/dt = 0$ corresponds to the thermodynamical equilibrium value $\eta = \eta_0(c,T)$ determined by the minimum of f condition $(\partial f/\partial \eta)_c \equiv f_\eta = 0$, as it should be. These equations also show that the time τ_0 for relaxation to this equilibrium value is of the order of that for one intersite atomic exchange, $\tau_0 \sim 1/\gamma_0^{12}$, in accordance with the considerations of AC.[1] Let us also note that the uniform ordering kinetics was discussed in more detail by Gschwend *et al.*[19] with the use of a cluster-type approximation, more sophisticated than the MFKE.

In the discussion of nonuniform fluctuations with $\mathbf{k} \neq 0$ we suppose for simplicity that partial equilibrium in the long-range order parameter η has been achieved: $\eta = \eta_0(c,T)$. As mentioned in Sec. I (and as seen from the results below), this is true, for example, for the long-wave fluctuations corresponding to concentration variations. Writing the wave amplitudes in (7) as $\delta c_{\mathbf{k}} = \delta c_{\mathbf{k}}^0 \exp(pt)$, $\delta \eta_{\mathbf{k}} = \delta \eta_{\mathbf{k}}^0 \exp(pt)$, we obtain after manipulations the following set of equations for $\delta c_{\mathbf{k}}^0$ and $\delta \eta_{\mathbf{k}}^0$

$$[A_{cc}(\mathbf{k}) - p]\delta c_{\mathbf{k}}^0 + A_{c\eta}(\mathbf{k})\delta \eta_{\mathbf{k}}^0 = 0, \tag{12a}$$

$$A_{\eta c}(\mathbf{k})\delta c_{\mathbf{k}}^0 + [A_{\eta\eta}(\mathbf{k}) - p]\delta \eta_{\mathbf{k}}^0 = 0. \tag{12b}$$

Here the matrix with coefficients $A_{\alpha\beta}(\mathbf{k})$ generalizes the right-hand side (RHS) of Eq. (2a) to the two-sublattice case under consideration:

$$A_{cc}(\mathbf{k}) = -\frac{1}{2}[(m_{12}\gamma_{0\mathbf{k}}^{12} + m_{11}\gamma_{0\mathbf{k}}^{11})d_{1\mathbf{k}} + (m_{12}\gamma_{0\mathbf{k}}^{12} + m_{22}\gamma_{0\mathbf{k}}^{11})d_{2\mathbf{k}}], \tag{13}$$

$$A_{c\eta}(\mathbf{k}) = -\frac{1}{2}[(m_{12}\gamma_{0\mathbf{k}}^{12} + m_{11}\gamma_{0\mathbf{k}}^{11})\tilde{d}_{1\mathbf{k}} - (m_{12}\gamma_{0\mathbf{k}}^{12} + m_{22}\gamma_{0\mathbf{k}}^{11})\tilde{d}_{2\mathbf{k}}],$$

$$A_{\eta c}(\mathbf{k}) = -\frac{1}{2}\{[m_{12}(\gamma_0^{12} + \gamma_{\mathbf{k}}^{12}) + m_{11}\gamma_{0\mathbf{k}}^{11}]d_{1\mathbf{k}} - [m_{12}(\gamma_0^{12} + \gamma_{\mathbf{k}}^{12}) + m_{22}\gamma_{0\mathbf{k}}^{11}]d_{2\mathbf{k}}\},$$

$$A_{\eta\eta}(\mathbf{k})=-\frac{1}{2}\{[m_{12}(\gamma_0^{12}+\gamma_{\mathbf{k}}^{12})+m_{11}\gamma_{0\mathbf{k}}^{11}]\tilde{d}_{1\mathbf{k}}$$
$$+[m_{12}(\gamma_0^{12}+\gamma_{\mathbf{k}}^{12})+m_{22}\gamma_{0\mathbf{k}}^{11}]\tilde{d}_{2\mathbf{k}}\},$$

where $d_{1\mathbf{k}}=z_1+\varphi_{\mathbf{k}}$, $d_{2\mathbf{k}}=z_2+\varphi_{\mathbf{k}}$, $\tilde{d}_{1\mathbf{k}}=z_1+\tilde{\varphi}_{\mathbf{k}}$, and $\tilde{d}_{2\mathbf{k}}=z_2+\tilde{\varphi}_{\mathbf{k}}$, with $z_1=1/c_1c_1'$, $z_2=1/c_2c_2'$ and $\varphi_{\mathbf{k}}=\beta v_{\mathbf{k}}$, while $\gamma_{0\mathbf{k}}^{12}=\gamma_0^{12}-\gamma_{\mathbf{k}}^{12}$ and $\gamma_{0\mathbf{k}}^{11}=\gamma_0^{11}-\gamma_{\mathbf{k}}^{11}$. The factors $m_{\alpha\beta}$ determine the c,η dependence of mobilities, similarly to m in Eq. (2b):

$$m_{12}=(c_1c_2c_1'c_2')^{1/2}\exp(\beta u_0 c),$$
$$m_{11}=c_1c_1'\exp[\beta(u_0c+\tilde{u}_0\eta)],$$
$$m_{22}=c_2c_2'\exp[\beta(u_0c-\tilde{u}_0\eta)]. \quad (14)$$

In deriving Eqs. (13) and (14) we took into account the equivalence of sublattices 1 and 2, as well as the partial equilibrium in the order parameter η, i.e., vanishing RHS in Eq. (9).

Two possible values of the increment, $p_+(\mathbf{k})$ and $p_-(\mathbf{k})$, are determined from the solubility condition for system (12):

$$p_\pm(\mathbf{k})=B_{\mathbf{k}}\pm(B_{\mathbf{k}}^2-D_{\mathbf{k}})^{1/2}, \quad (15)$$

where $B_{\mathbf{k}}=(A_{cc}+A_{\eta\eta})/2$, and $D_{\mathbf{k}}=A_{cc}A_{\eta\eta}-A_{c\eta}A_{\eta c}$.

The explicit expression for $D_{\mathbf{k}}$ is relatively simple. It factorizes into two factors, the ''kinetic'' one $M_{\mathbf{k}}$ that depends on the functions $m_{\alpha\beta}$ and $\gamma_{\mathbf{k}}^{\alpha\beta}$, and the ''thermodynamic'' one $\Delta_{\mathbf{k}}$ that depends on the reduced interactions $\varphi_{\mathbf{k}}$ and $\tilde{\varphi}_{\mathbf{k}}$ and can also be expressed in terms of the derivatives of the free energy f in (10) over c or η:

$$D_{\mathbf{k}}=M_{\mathbf{k}}\Delta_{\mathbf{k}}, \quad (16a)$$

$$M_{\mathbf{k}}=m_{12}^2\gamma_{0\mathbf{k}}^{12}(\gamma_0^{12}+\gamma_{\mathbf{k}}^{12})+m_{12}(m_{11}+m_{22})\gamma_{0\mathbf{k}}^{11}\gamma_0^{12}$$
$$+(m_{12}\gamma_{0\mathbf{k}}^{11})^2, \quad (16b)$$

$$\Delta_{\mathbf{k}}=\frac{1}{2}(d_{1\mathbf{k}}\tilde{d}_{2\mathbf{k}}+d_{2\mathbf{k}}\tilde{d}_{1\mathbf{k}})=f_{cc}^a f_{\eta\eta}+f_{\eta\eta}\varphi_{\mathbf{k}0}+f_{cc}\tilde{\varphi}_{\mathbf{k}0}$$
$$+\varphi_{\mathbf{k}0}\tilde{\varphi}_{\mathbf{k}0}. \quad (16c)$$

Here $\tilde{\varphi}_{\mathbf{k}0}=\tilde{\varphi}_{\mathbf{k}}-\tilde{\varphi}_0$, $f_{cc}^a=f_{cc}-f_{c\eta}^2/f_{\eta\eta}$ is the full concentrational derivative of the adiabatic (or ''conditional''[1]) free energy $f^a=f[c,\eta_0(c)]$, $f_{cc}^a=d^2f^a/dc^2$, found by taking into account the condition $f_\eta=0$ at $\eta=\eta_0(c)$, and f_{cc}, $f_{\eta\eta}$, and $f_{c\eta}$ are the formal partial derivatives of the function $f(c,\eta)$ in (10) at $\eta=\eta_0(c)$:

$$f_{cc}=\left(\frac{\partial^2 f}{\partial c^2}\right)_\eta=z_+ +\varphi_0, \quad f_{\eta\eta}=\left(\frac{\partial^2 f}{\partial \eta^2}\right)_c=z_+ +\tilde{\varphi}_0,$$
$$f_{c\eta}=\frac{\partial^2 f}{\partial c\,\partial\eta}=z_-, \quad (17)$$

where $z_\pm=\frac{1}{2}(z_1\pm z_2)$. The explicit expression for $B_{\mathbf{k}}$ in (15) is more cumbersome:

$$B_{\mathbf{k}}=-m_{12}[\gamma_0^{12}(f_{\eta\eta}+\tilde{\varphi}_{\mathbf{k}0})+\tfrac{1}{2}\gamma_{0\mathbf{k}}^{12}(\varphi_{\mathbf{k}}-\tilde{\varphi}_{\mathbf{k}})]$$
$$-\tfrac{1}{4}\gamma_{0\mathbf{k}}^{11}[(m_{11}+m_{22})(f_{cc}+f_{\eta\eta}+\varphi_{\mathbf{k}0}+\tilde{\varphi}_{\mathbf{k}0})$$
$$+(m_{11}-m_{22})(z_1-z_2)]. \quad (18)$$

Relations (12)–(18) provide the general solution for the stability problem. The relations can be simplified if one accepts the usual assumption that the intersite atomic exchange is dominated by the nearest-neighbor jumps of atoms in the crystal lattice. For example, for the $B2$ phase this implies that the quantities $\gamma_{\mathbf{k}}^{11}$ in Eqs. (13) and (16) can be neglected as compared to $\gamma_{\mathbf{k}}^{12}$, so that $M_{\mathbf{k}}$ and $B_{\mathbf{k}}$ reduce to the first terms in Eqs. (16b) and (18) only.

Let us discuss the signs of the derivatives $f_{\eta\eta}$, f_{cc}, and f_{cc}^a in Eqs. (16)–(18). The derivative $f_{\eta\eta}$ is positive for all $\eta_0\neq 0$, i.e., for all $T<T_{\rm os}(c)$, as the ''partial equilibrium'' value $\eta=\eta_0(c)$ corresponds to the minimum of $f(c,\eta)$ over η. When the c,T point under consideration approaches the ordering spinodal $T_{\rm os}(c)$, both $\eta_0(c)$ and $f_{\eta\eta}(c,T)$ tend to zero, since the curve $T_{\rm os}(c)$ is determined by the equation $f_{\eta\eta}=0$ at $\eta=0$. The difference $f_{cc}-f_{\eta\eta}$ according to Eq. (17) is $\varphi_0-\tilde{\varphi}_0$, and is thus positive; otherwise SD into two disordered phases would take place rather than alloy ordering. Therefore, the quantity f_{cc} is positive, too, and it is generally not small. The conditional spinodal $T_{\rm cs}(c)$ is determined by the equation $f_{cc}^a=0$, so that f_{cc}^a is negative at $T<T_{\rm cs}$, i.e., in region (d) of Fig. 1, and it is positive at $T>T_{\rm cs}$. Thus the product $f_{cc}^a f_{\eta\eta}$ in Eq. (16c) is negative in area (d) of Fig. 1, and it vanishes at either borderline of this area, $T_{\rm os}(c)$ and $T_{\rm cs}(c)$.

For simplicity below we consider only long-wave fluctuations with small k, as in most treatments of SD in disordered alloys.[7,11] Let us first discuss the physical meaning of two fluctuation modes in Eqs. (12), corresponding to $p=p_+$ and $p=p_-$, in the limit $k\to 0$. In this limit Eq. (12b) takes the form

$$f_{\eta c}\delta c_\pm+(f_{\eta\eta}+p_\pm/2m_{12}\gamma_0^{12})\delta\eta_\pm=0 \quad (19)$$

where the index + or − marks the mode with $p=p_+$ or $p=p_-$. The expressions for p_- and p_+ at $k\to 0$ are

$$p_-=-2m_{12}\gamma_0^{12}f_{\eta\eta}, \quad (20a)$$
$$p_+=(-f_{cc}^a)M'k^2. \quad (20b)$$

Here $M'k^2$ is the small-k expansion for the sum $\gamma_{0\mathbf{k}}^{12}m_{12}+\gamma_{0\mathbf{k}}^{11}(m_{11}+m_{22})/2$, which generalizes the similar expansion in Eq. (5) to the case $\eta\neq 0$.

Equations (19) and (20a) show that in the ''minus'' mode, the concentrational amplitude δc_- vanishes. Therefore, this mode describes the uniform relaxation of the order parameter η at the ''frozen'' concentration c, and the value p_-, Eq. (20a), corresponds just to linearizing the relevant equation

(11) in the small difference $\delta\eta_- = \eta - \eta_0(c)$. On the contrary, the ''plus'' mode describes the diffusion of concentration. At T higher than the ordering spinodal $T_{os}(c)$ it corresponds to the relaxation of fluctuations, while at $T<T_{os}(c)$ it describes the uphill diffusion corresponding to SD. For $k\to 0$ (the case under consideration here) diffusion occurs adiabatically slowly, and relation (19) between δc_+ and $\delta\eta_+$ corresponds to varying the concentration along the ''adiabatic'' partial equilibrium line $f_\eta = 0$: $f_{\eta c}\delta c_+ + f_{\eta\eta}\delta\eta_+ = 0$.

To study SD at finite k, in particular, at $k=k_c$ corresponding to critical waves, one should keep higher powers of k^2 in the small-k expansions of Eqs. (12)–(18). The increment $p_+(k)$ takes the form

$$p_+(k) = m_{12}\gamma_0^{12}\{[(f_{\eta\eta}+\lambda k^2)^2 - 2\mu k^2(f_{cc}^a f_{\eta\eta} + \nu k^2)]^{1/2} - (f_{\eta\eta}+\lambda k^2)\}. \quad (21)$$

Here $\mu = M'/m_{12}\gamma_0^{12}$, while λk^2 or νk^2 corresponds to the small-k expansion of $B_{\mathbf{k}}$ or $\Delta_{\mathbf{k}}$ in Eq. (18) or (16b):

$$\lambda k^2 = \{\tilde{\varphi}_{\mathbf{k}0} + [\gamma_{0\mathbf{k}}^{12}(f_{cc}-f_{\eta\eta}) + \gamma_{0\mathbf{k}}^{11} f_{cc}]/2\gamma_0^{12}\}_{k\to 0}, \quad (22a)$$

$$\nu k^2 = (\tilde{\varphi}_{\mathbf{k}0} f_{cc} + \varphi_{\mathbf{k}0} f_{\eta\eta})_{k\to 0}. \quad (22b)$$

Explicit expressions for the wave number $k=k_c$ and the increment $p=p_c$ of critical waves can be found from Eq. (21) and the condition of p_+ maximum: $\partial p_+/\partial k = 0$. These expressions can be simplified if one takes into account the fact that k_c is small (and the small-k expansion used above is valid) only if either f_{cc}^a or $f_{\eta\eta}$ is small, i.e., if the c,T point under consideration is close to either the conditional or the ordering spinodal in Fig. 1. We consider below these two particular cases.

(i) *Point c,T is close to the conditional spinodal*. Here f_{cc}^a is small, k_c^2 is proportional to f_{cc}^a, and the RHS of Eq. (21) can be expanded in k^2. Then expressions for $p_+(k)$, k_c, and p_c become similar to Eqs. (5) and (6) for disordered alloys, differing only by the replacement of f_{cc} by f_{cc}^a and by the presence of renormalizing factors:

$$k_c^2 = (-f_{cc}^a)f_{\eta\eta}/2\nu, \quad p_c = M'(f_{cc}^a)^2 f_{\eta\eta}/4\nu. \quad (23)$$

To make Eqs. (23) more transparent, we also express the coefficient ν in terms of the mean interaction lengths x_v and $\tilde{x}_v$ for the interaction potentials v and $\tilde{v}$. Supposing for simplicity both the ordered and disordered phases to be cubic (as is the case for $B2$ ordering on the bcc lattice), we define x_v and $\tilde{x}_v$ by

$$x_v^2 = \frac{1}{3v_0}\sum_{\mathbf{r}} v(\mathbf{r})r^2, \quad \tilde{x}_v^{\,2} = \frac{1}{3\tilde{v}_0}\sum_{\mathbf{r}} v(\mathbf{r})e^{i\mathbf{k}_s\mathbf{r}}r^2. \quad (24)$$

Then expression (22b) for ν can be written as

$$\nu = 2\beta T_c(f_{cc}\tilde{x}_v^{\,2} + f_{\eta\eta}\rho x_v^2), \quad (25)$$

where $\rho = v_0/\tilde{v}_0$, and we use the MFA relation $T_c = -\tilde{v}_0/4$ for the critical ordering temperature T_c.

Let us discuss the sign of ν in Eq. (25). As mentioned, $f_{cc} > f_{\eta\eta}$, and the presence of a tricritical point in the phase diagram implies that the ratio ρ lies within the interval[9] $-1/2<\rho<1$. Therefore, for usual interaction potentials with $x_v \sim \tilde{x}_v$, ν is positive: This was implicitly assumed in writing Eqs. (23). However, if for some specific system the quantity ν turns out to be negative [which in our model would correspond to small values of $(\tilde{x}_v/x_v)$ and $\rho<0$], then increment $p_+(k)$, Eq. (21), for finite k is positive even at $T>T_{cs}(c)$, i.e., in region (e) of Fig. 1. This implies an instability of the homogeneous ordered state and a tendency to the formation of an incommensurate phase in this area; in the present work we will not address this exotic possibility.

For the normal case $\nu>0$, Eqs. (23) show that at small distances ζ between the point c,T and the conditional spinodal $T_{cs}(c)$, the values of $k_c(\zeta)$ and $p_c(\zeta)$ vary with ζ similarly to those in Eqs. (6) for SDDA: $k_c \sim \zeta$, $p_c \sim \zeta^2$. Therefore, the effect of ordering on the kinetic characteristics reduces here to the appearance of some renormalization factors in Eqs. (23) as compared with (6).

(ii) *Point c,T is close to the ordering spinodal*. Here the derivative $f_{\eta\eta}$ is small (while f_{cc}^a can be not small), $k_c^2 \sim f_{\eta\eta}$, and at $k\sim k_c$ all terms in Eq. (21) have the same order of magnitude. The dependence $p_+(k)$ becomes more complex than in (5). The expressions for k_c and p_c can be written as

$$k_c^2 = f_{\eta\eta}[(1+\alpha)^{1/2}-1]\frac{T}{2T_c\tilde{x}_v^2}, \quad (26a)$$

$$p_c = m\gamma_0^{12} f_{\eta\eta} f_{cc}[2+\alpha-2(1+\alpha)^{1/2}]\frac{Tx_\gamma^2}{4T_c\tilde{x}_v^2}. \quad (26b)$$

Here m is the same as in (2b), while quantities α and x_γ are defined by the relations

$$\alpha = -f_{cc}^a/f_{cc}, \quad x_\gamma^2 = \sum_{\mathbf{r}} \gamma(\mathbf{r})r^2/3\gamma_0^{12}. \quad (27)$$

In the derivation of Eqs. (26) we supposed the ratio $x_\gamma^2/\tilde{x}_v^2$ to be small, as the ''mean atomic jump distance'' x_γ in (27) is of the order of the intersite distance r_{nn}, while the formal condition for the applicability of the MFA implies the inequality $\tilde{x}_v^2 \gg r_{nn}^2$.[13,12]

Equations (26) show that near the ordering spinodal the kinetic characteristics of SD differ markedly from those for the disordered alloy, unlike case (i) discussed above. This is due to the strong coupling between fluctuations of c and η at small values of η_0. In particular, the maximal increment p_c here varies linearly with the distance ζ from c,T to the ordering spinodal $T_{os}(c)$, instead of the quadratic dependence in Eq. (6) or (23). Thus critical fluctuations here grow much faster than those under SDDA with a similar distance ζ to the spinodal.

Near the tricritical point both f_{cc}^a and $f_{\eta\eta}$ become small, and Eqs. (23) and (26) turn into each other. Explicit expressions for k_c and p_c here can be obtained setting in Eqs. (23): $\nu = 2\beta T_c f_{cc}\tilde{x}_v^2$, $M' = m\gamma_0^{12}x_\gamma^2/2$. If we denote the distance from the point c,T to the conditional and ordering spinodal as ζ_{cs} and ζ_{os}, respectively, then k_c and p_c in this area vary

with ζ_{cs} and ζ_{os} as $k_c \sim \zeta_{cs}\zeta_{os}$, $p_c \sim \zeta_{cs}^2\zeta_{os}$. Therefore, the critical fluctuations here have a large wavelength and grow with time very slowly.

The above analysis shows that the presence of a strong coupling between the fluctuations of concentration and degree of order results in a number of peculiarities in the kinetic characteristics of SD under ordering. Below we show that the possibility of APB's to be present in the initial state can lead to additional specific effects in the kinetics of such SD.

III. MICROSTRUCTURAL EVOLUTION IN THE COURSE OF DECOMPOSITION WITH ORDERING

In this section we investigate transient morphologies arising under alloy decomposition with ordering. Let us note that experimentally such morphologies can be studied directly, taking advantage of dark-field images in transmission electron microscopy. This type of observation can provide richer information, in particular, for comparison with results of the present study, than structural factors $S(\mathbf{k},t)$ as measured by standard diffraction experiments. This was demonstrated, in particular, by experiments in Refs. 1 and 2 for FeAl alloys. Therefore, comparison of the theoretical results for microstructural evolution under SD in ordered and disordered alloys, being combined with experimental studies of SD under ordering, can provide significant information about the adequacy of the currently used models of SD.[20]

In the present study we use computer simulations based on the MFKE (1). For simplicity and convenience of presentation, we consider the same two-dimensional (2D) model on the square lattice as CK,[3–5] at the same temperature $T=0.424T_c$, where T_c is the critical ordering temperature, and the same or similar compositions c equal to 0.175, 0.25, 0.325, or 0.415. The as-quenched states corresponding to these c,T points will be called for brevity the α, β, γ, or δ state; see Fig. 1. The asymmetric potential u for this model is zero, while the configurational interactions $v(\mathbf{r})$ for first, second, and third neighbors are $v_1=1$, $v_2=-0.8$, and $v_3=-0.5$. The intersite atomic jumps are supposed to occur only between nearest neighbors, $\gamma(\mathbf{r})=\gamma_{nn}$, and we use the ''reduced'' time variable $t'=t\gamma_{nn}$. The superstructure vector $\mathbf{k}_s$ for the ordered 2D ''$B2$ phase'' is $(1/2,1/2)2\pi/a$, and the perfectly ordered state corresponds to $c_{ord}=1/2$. In accordance with the ''lever rule,'' the portion x_{ord} of the ordered phase in the two-phase alloy (at moderate temperatures under consideration) can be estimated as $x_{ord}\simeq 2c$. Therefore, the results of the present simulations for $c=c_\alpha=0.175$ ($x_{ord}\simeq 0.35$) and $c=c_\gamma=0.325$ ($x_{ord}\simeq 0.65=1-0.35$) can be naturally compared with those for SDDA at $c=0.35$ presented in Ref. 10. The extension of the MFKE-based computer simulations to three-dimensional lattices, such as the bcc or fcc ones, does not present any difficulty, as was demonstrated, e.g., in Ref. 9.

Keeping in mind the comparison with Refs. 3–5, we first consider SD in the absence of APB's (i.e., in the case $l \gg \lambda_c$), since the presence of APB's brings about certain peculiarities in the microstructural evolution. For state γ, such ''homogeneous'' SD (HSD) can be realized if the alloy has been annealed prior to quench in some state in area (b).[1,2]. Then we investigate quenches (a)→(d) in a more typical case $l \lesssim \lambda_c$, i.e., in the presence of APB's. We show that the transient morphologies sharply change when the c,T point is shifted from left to right in area (d): for states α, β, and γ the morphologies are quite different. Finally, we discuss quench (a)→(e) and show that nucleation on APB's results in specific features of evolution.

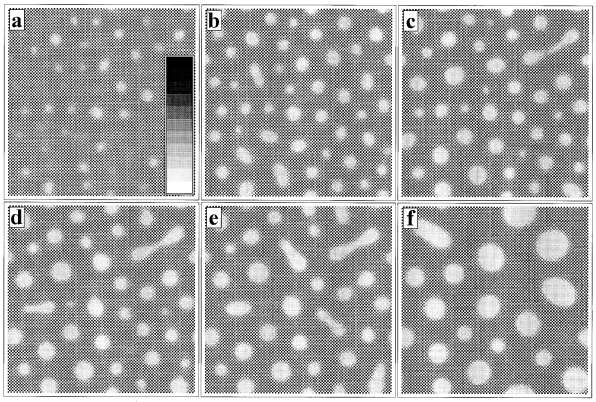

FIG. 2. Temporal evolution of mean occupations $c_i=c(\mathbf{r}_i)$ for the alloy model used under spinodal decomposition of a single-domain ordered state, at $T'=T/T_c=0.424$, $c=0.325$, and the following values of reduced time $t'=t\gamma_{nn}$: (a) 500, (b) 1000, (c) 2000, (d) 2500, (e) 3000, and (f) 10 000. The insert in (a) shows the relation between the darkness level and c_i values, which vary linearly from 0 to 1 with the distance from bottom to top.

The simulations have been made on a square lattice of 128×128 sites with periodic boundary conditions. The simulation methods were the same as in Refs. 10 and 9. The as-quenched distribution $c_i(0)$ was characterized by its mean value c and small random fluctuations δc_i; usually we used $\delta c_i=\pm 0.01$. In simulations of HSD we also imposed the initial uniform ordering $\eta(0)=0.04$, to create a single-domain state.

The results of our simulations are illustrated in Figs. 2–6. Below we discuss them, indicating for each simulation (i) the type of quench, (ii) the type of initial ordering, i.e., the presence of a single or of several AP domains, which will be abbreviated as the ''HSD,'' ''SD with APB's,'' or ''nucleation with APB's'' case, respectively, and (iii) the initial composition c. The reduced temperature $T'=T/T_c$ in all simulations is 0.424.

(3.1) (b)→(d); HSD, $c=c_\gamma=0.325$, Fig. 2. The state γ in Fig. 1 is close to the conditional spinodal; i.e., the distance ζ between point γ and $T_{cs}(c)$ is small. As mentioned in Sec. II, the kinetic characteristics of the Cahn stage of SD, $p(k)$, $k_c(\zeta)$, and $p_c(\zeta)$, are, in this case, similar to those for SDDA. Thus it is natural to expect that also for the later (i.e., coarsening) stages of SD, the evolution type will be similar to that for SDDA.

It was mentioned earlier[10] that precipitation and coarsening processes under SDDA can usually be divided into three stages.

(A) The ''droplet formation'' stage, where Cahn concentration waves begin to coalesce, and primary precipitates, or ''droplets,'' are formed.

(B) The ''coagulation'' or ''fusion'' stage, where the dominant mechanism for droplet growth is their coalescence via the ''bridge'' mechanism discussed in Ref. 10.

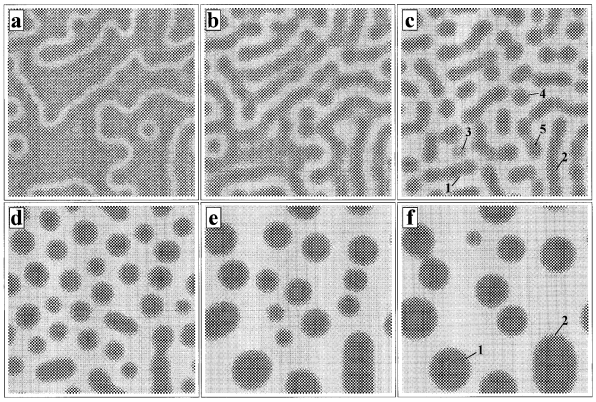

FIG. 3. Temporal evolution of $c_i = c(\mathbf{r}_i)$ after quenching the alloy from a disordered state with randomly distributed fluctuations $\delta c_i = \pm 0.01$ to $T' = 0.424$, at $c = 0.175$ and following t': (a) 50, (b) 100, (c) 200, (d) 1000, (e) 4000, and (f) 9000.

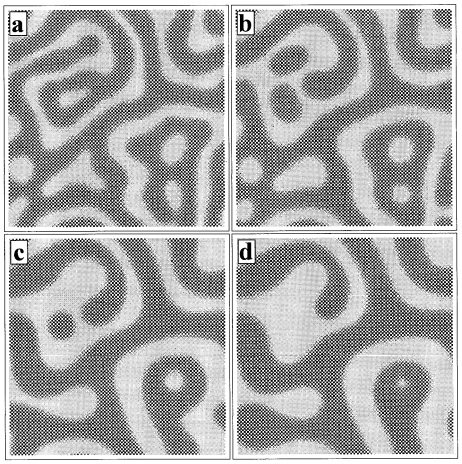

FIG. 4. Same as in Fig. 3, but at $c = 0.25$ and following t': (a) 1000, (b) 2000, (c) 4000, and (d) 6000.

(C) The final stage, where coarsening is dominated by the evaporation-condensation (EC) mechanism,[14] by which larger droplets grow owing to the evaporation of smaller ones.

In simulations of SDDA at $c = 0.35$ (Ref. 10) the division into stages (A), (B), and (C) was found to be rather clear.

The similar division has been revealed in the present simulation of HSD of the state γ. Stage (A) here approximately corresponds to the time interval $300 < t' < 1000$. Figure 2(a) illustrates the formation of an approximately periodic array of minima of $c(\mathbf{r})$ via the superposition of nonlinear critical waves with $\lambda \simeq \lambda_c$; this distribution is analogous to the ''hill-like'' profile of $c(\mathbf{r})$ shown in Fig. 1 in Ref. 10. Stage (B) approximately corresponds to the time interval $1000 < t' < 4000$, when 14 droplets out of 48 coalesce, and 7 evaporate; and stage (C), to $t' > 4000$: For $4000 < t' < 10000$, 3 droplets out of 27 coalesce and 6 evaporate. These mechanisms are illustrated in Figs. 2(c)–2(f) where both fusion and evaporation processes can be seen. Note, in particular, the double fusion of three droplets in the upper right part of Fig. 2(c), realized via the formation of two bridges with a length of the order of the droplet diameters. However, the borderline between stages (B) and (C) under this SD is less distinct than that for SDDA in Ref. 10. For example, during $t' = 2000$–4000, 8 droplets coalesce and 5 evaporate; i.e., both mechanisms make similar contributions to coarsening, while Fig. 2(f) shows a fusion event that happened at rather large $t' \simeq 9000$, when the EC mechanism is generally dominant.

(3.2) (a)→(d), SD with APB's, $c = c_\alpha = 0.175$, Fig. 3. As mentioned in Sec. I, due to the depletion of both the order parameter and the alloy minority component within the APB the latter can act as an embryo for the disordered phase at phase separation. Under SD, the presence of such embryos induces the formation of critical concentration waves that replicate the initial APB shape and have periods $\lambda \sim \lambda_c$. This APB replication phenomenon is discussed in more details in Sec. IV. As a consequence, at the beginning of stage (A) the concentration $c(\mathbf{r})$ and the order parameter $\eta(\mathbf{r})$ profiles have a ''ridge-valley''-like pattern, rather than the hill-like one observed for SDDA.[10] This is illustrated by Figs. 3(a) and 3(b) and results in a significant difference in microstructure of stage (A) as compared to that for HSD discussed above [point (3.1) above].

Stage (A) now approximately corresponds to $t' = 50$–300, being accelerated as compared to HSD (3.1) by the presence of APB's as embryos for the decomposition. Figures 3(b)–3(d) show that the formation of droplets from initial stripes with enhanced concentration $c(\mathbf{r})$ proceeds via two mechanisms: (i) splitting of these stripes into shorter pieces that later on spheroidize [see, e.g., droplets 1 and 2 in Figs. 3(c)–3(f)], and (ii) ''consumption'' of some of these new-born droplets by their neighbors via the bridge mechanism discussed in Ref. 10. The latter occurs for droplet 3 in Fig. 3(c), and it also happens for droplets 4 and 5 at $t' \simeq 750$.

As soon as $t' = 1000$, the microstructure shown in Fig. 3(d) does not differ qualitatively anymore with that for HSD in Fig. 2(d). However, the coagulation stage (B) now is relatively short: It lasts approximately for $t' = 300$–1000, when 9 droplets among 43 coalesce and none evaporates. At $t' > 1000$, the EC mechanism becomes dominant: For $t' = 1000$–$10\,000$, only 3 droplets coalesce while 22 evaporate. This stage (C) is illustrated by Figs. 3(e) and 3(f); the latter figure also shows one of the rare fusion events for this stage.

(3.3) (a)→(d), SD with APB's, $c = c_\beta = 0.25$, Fig. 4. Microstructural evolution at $c = 0.25$ under HSD (i.e., in the absence of APB's) is similar to that under SDDA at $c = 1/2$ shown, for example, in Ref. 21 so that we do not describe it here. The presence of APB's brings about new features in the evolution. Unlike the case of $c = 0.175$ discussed in simulation (3.2), the initial ''APB-replicated'' structure here is not destroyed for a short time $t' \lesssim 100$, but is clamped by the precipitation of the disordered phase. Comparison of Fig. 3(a) with Fig. 4(a) or 4(b) shows that the structure is basically preserved up to significant times ($t' \gtrsim 2000$). As the proportion of both phases in the mixture is similar, $x_{\mathrm{ord}} \sim x_{\mathrm{disord}} \sim 1/2$, the evolution is mainly realized via the growth of initially ordered and disordered layers and the formation of droplets of either phase within the other one. Later on the droplets evaporate [Figs. 4(c) and 4(d)], and the morphology begins to evolve to that of interconnected interpenetrating domains characteristic of SDDA at $c = 1/2$.[21]

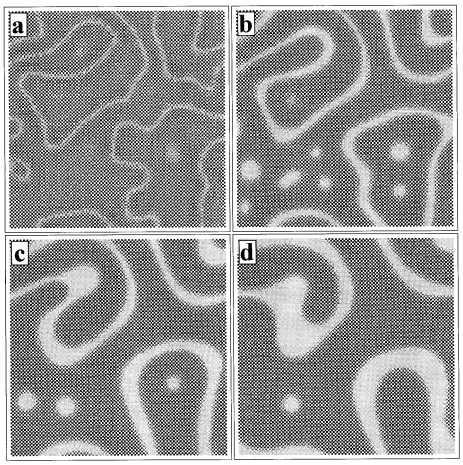

FIG. 5. Same as in Fig. 3, but at $c=0.325$ and following t': (a) 50, (b) 1000, (c) 3500, and (d) 10 000.

(3.4) (a)→(d), SD with APB's, $c=c_\gamma=0.325$, Fig. 5. Unlike for HSD, an approximate topological symmetry between SD of states α and γ in the presence of APB's [compare Figs. 3(a) and 5(a)] is observed at early stages only ($t'\lesssim 50$). Later on at larger $c=c_\gamma=0.325$, the initial APB becomes a center of precipitation that clamps its contour (as was the case for $c=0.25$), while at relatively small $c=c_\alpha=0.175$, APB's coalesce to form a continuous disordered phase around the ordered droplets. Figures 5(a)–5(d) show that precipitate growth at APB's occurs due to the evaporation of isolated droplets; as a consequence APB's thicken and play the role of ''larger droplets'' in the EC mechanism. Further evolution of these precipitates to single-connected ones is similar to that shown in Fig. 6 below and needs considerable time $t'\gtrsim(2-3)\times 10^4$. Until this final stage is reached, the morphologies under such SD are quite different from those under HSD (i.e., in the absence of APB's) with the same $c=0.325$ (Fig. 2).

(3.5) (a)→(e), nucleation with APB, $c=c_\delta=0.415$, Fig. 6. In area (e) decomposition only proceeds via nucleation and growth, and APB's become embryos of the disordered phase. As there is no spinodal instability here, local concentration fluctuations do not grow with time, and no APB replication occurs either. Thus the number of initial disordered droplets here is significantly less than under SD, which is seen from comparison of Fig. 5(a) or 5(b) with Figs. 6(a)–6(c). The only mechanism for creating such droplets (in the MFA used that neglects thermal fluctuations in occupation numbers[12,13]) is the possible collapse of AP domains.[9] For illustrating this mechanism, the simulation shown in Fig. 6 was started with an initial distribution of fluctuations δc_i (different from that in other simulations) chosen to generate several initial AP domains of comparable size. The primary AP domain structure is established after a short time $t'\sim 1$; later APB's begin to move, mainly to shrink in order to decrease the interface energy. Whenever an antiphase domain has a time to collapse before the precipitation on its APB damps its motion, near the collapse point both the order parameter and the alloy minority concentration are depleted, and this area becomes an embryo for the disordered phase.[9] This is illustrated in Fig. 6(c): Droplets 1 and 2 originate from the collapses of AP domains 1 and 2 in Fig. 6(b).

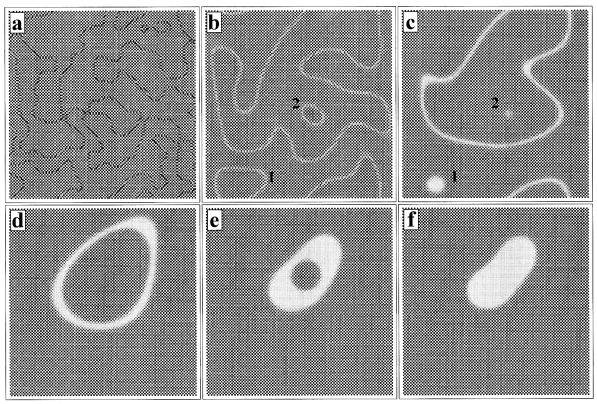

FIG. 6. Same as in Fig. 3, but at $c=0.415$ and following t': (a) 1, (b) 10, (c) 1000, (d) 9000, (e) 23 000, and (f) 25 000.

Later on these droplets evaporate with condensation on precipitates formed at APB's. Further stages illustrated by Figs. 6(d)–6(f) correspond to the evolution from initial APB-shaped precipitates to more compact, single-connected ones. It is realized, first, via smoothening the most curved parts of the contour [see Figs. 6(c) and 6(d)], and then via shrinkage and thickening of a disordered shell embracing the inner ordered area, due to diffusion of atoms from this area across the shell. In the course of the process the inner droplet becomes almost spherical [Fig. 6(e)], and finally evaporates. As the total time t'_t for this process is determined by diffusion along or across APB's, it should vary with the initial AP domain size l approximately quadratically: $t'_t\sim l^2$.

Now let us compare our simulation results with those of CK (Refs. 3–5) for the same model. As mentioned in Sec. I, CK used the partially linearized kinetic equation (PLKE) instead of the full MFKE; therefore, the comparison can provide information on errors brought about by the ''partial linearization'' of MFKE in describing the alloy evolution. CK made their simulations for the quench discussed in point (3.2) above, using lattices of 64×64 and 128×128 sites,[3–5] and also for quenches discussed in points (3.3) and (3.5), using a lattice of 64×64 sites. Their PLKE corresponds to replacing the occupation-dependent terms $\gamma_{is}c'_i c_s$ and $\gamma_{is}c'_s c_i$ in (1) by a constant L_1. To have coincident results at early times $t\to 0$ (where linearization of the MFKE is justified), we should put $L_1=\gamma_{\rm nn}cc'$ with c and c' corresponding to the initial homogeneous alloy. It implies that our reduced time $t'=\gamma_{\rm nn}t$ is related to $t^*=L_1 t$ in CK by $t'=t^*/cc'$.

The comparison of our results with Refs. 3–5 reveals the following differences.

(i) In simulation (3.2), there is a significant distortion of the time scale in the PLKE relative to the MFKE: Evolution in the PLKE occurs much more slowly. For example, Figs. 3(b) and 3(c) show fusion of initial APB's already at $t'=100-200$, while in Refs. 4 and 5 it begins only at $t^*\gtrsim 100$ (i.e., $t'\gtrsim 700$). For $t'\gtrsim 4000$, Fig. 3(e) demonstrates the advanced stage (C) of SD dominated by the EC mechanism, characterized by a significantly reduced number of droplets and large nonuniformity in their sizes and positions, while results of CK (Refs. 3–5) for $t^*=500$ and 1000 ($t'\simeq 3500$ and 8000) rather correspond to the beginning of

stage (B) ($t' \sim 1000$), with the presence of many small uniformly distributed droplets.

(ii) No discussion of the relative importance of the coagulation and EC mechanisms under SD (3.2) is presented in Refs. 3–5. However, results[4,5] for $t^* = 500$ ($t' \simeq 3500$) seem to show a great number of fusion processes, while in our analysis we mentioned the suppression of this mechanism for SD (3.2). Therefore, PLKE can also qualitatively distort the evolution mechanism.

(iii) Simulation (3.4) was made in Ref. 3 on a small lattice of 64×64 sites. Therefore, a detailed comparison with our results is hindered by the scarcity of droplets and probable effects of periodic boundary conditions in the work reported in Ref. 3. However, our Fig. 4 reveals a much more dispersed and nonuniform distribution of precipitates than that shown in Ref. 3 for $t^* = 200$ ($t' \simeq 1100$) and $t^* = 1000$ ($t' \simeq 5300$). It is not clear whether the discrepancy is due to errors of the PLKE or due to the small size of the simulation box in Ref. 3; the same thing can be said about the results discussed in point (iv) below.

(iv) The structural evolution under quench (3.5) in Ref. 3 is quite different from that shown in our Fig. 6. In particular, the final state $t^* = 500$ in Ref. 3 shows two straight ''frozen'' APB's, with no sign of further evolution: As we mentioned in point (3.5), decomposition in area (e) can be realized either via evaporation of small droplets (that are absent at $t^* = 500$ in Ref. 3), or via changes of the APB shape, which do not occur for straight APB's either. Thus the decomposition stage appears not to be reached in Ref. 3 for this simulation.

Therefore, the comparison of our results with those of Refs. 3–5 seems to imply that the PLKE can significantly distort the description of the microstructural evolution. However, a more detailed comparison is hindered by the scarcity of results presented in Refs. 3–5.

IV. REPLICATION OF ANTIPHASE BOUNDARIES UNDER SPINODAL DECOMPOSITION WITH ORDERING

As mentioned in Sec. I, the depletion of both the order parameter and the alloy minority component within APB's (Ref. 9) makes APB's possible embryos of the disordered phase under SD. In Sec. III we showed that after direct quench of a disordered alloy into area (d) in Fig. 1, the initial AP domains have usually small sizes $l \lesssim \lambda_c$, and transient morphologies under SD have a chaotic character. However, if before quenching into area (d) the alloy is annealed in the ordered phase (b), the AP domains grow, so that after the subsequent quench (b)→(d) the relation $l \gg \lambda_c$ can be satisfied. The APB's can then be well separated, and peculiar quasi-periodic structures replicating the initial form of the APB's can develop. Examples of such structures have been presented in Fig. 4 in Ref. 5 and in Fig. 1(c) in Ref. 22, but their physical origin and possible relevance to actual experiments have not been discussed.

To study this APB replication phenomenon, we simulated the above-mentioned two-step quench in our 2D model. First we annealed an initially disordered alloy for time t_a at temperature T_a corresponding to area (b) in Fig. 1, and then quenched the annealed alloy to the final temperature T in area (d). In our simulations we employed $t'_a = 100$,

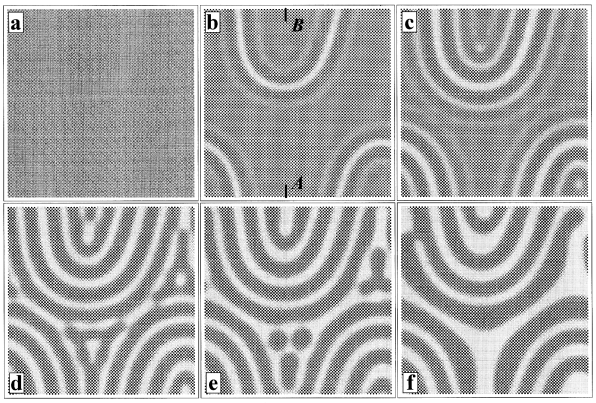

FIG. 7. Temporal evolution of the alloy model after the disordered state with $c = 0.26$ is annealed at $T'_a = T'_t = 0.753$ for $t' = 100$, and then quenched to $T' = 0.424$, for the following times t' after the quench: (a) 0 (as quenched), (b) 100, (c) 200, (d) 500, (e) 1000, and (f) 3000.

$T_a = T_t = 0.753 T_c$, and $T = 0.424 T_c$.

Our results are illustrated in Figs. 7–9. Figs. 7 and 8 show a well-defined replication of APB's. The mean local composition $\overline{c}(\mathbf{R})$ in Fig. 8 is obtained by averaging c_i over four sites of an elementary square in the 2D lattice.[9] As discussed earlier,[9] lowering the temperature to $T < T_a$ results in lowering the local concentration minimum within APB (''deepening the c well'').[9] As a consequence, the solute atoms expelled from the c well build the ''concentration bank'' (c bank) adjacent to this well. Since the alloy state is in the SD instability area, the c bank does not relax but rises with time, unlike the case treated in Ref. 9 where the alloy was in the stable ordered state. This increase in c requires an additional flow of solute atoms not only from the original c well where the concentration has been already depleted, but also from adjacent outer regions. As a result a second local minimum in $\overline{c}(\mathbf{R})$ appears, etc. Thus a wavelike distribution $\overline{c}(\mathbf{R})$ is spreading over the entire crystal, being accompanied with the relevant modulations of the local order parameter $\eta(\mathbf{R}) \simeq \eta_0[\overline{c}(\mathbf{R})]$. The distribution has a characteristic wavelength $\lambda \sim \lambda_c$, while its front replicates the initial APB form. Therefore, transient quasiperiodic structures arise.

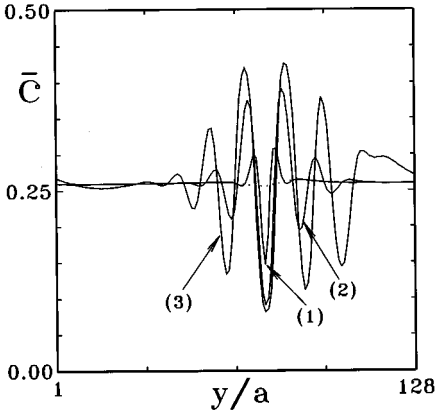

FIG. 8. Profile of the mean local composition $\overline{c}(\mathbf{R})$ along the vertical line AB indicated in Fig. 7(b). Dotted line, $t' = 0$. Solid curves, (1) $t' = 10$, (2) $t' = 100$, and (3) $t' = 200$.

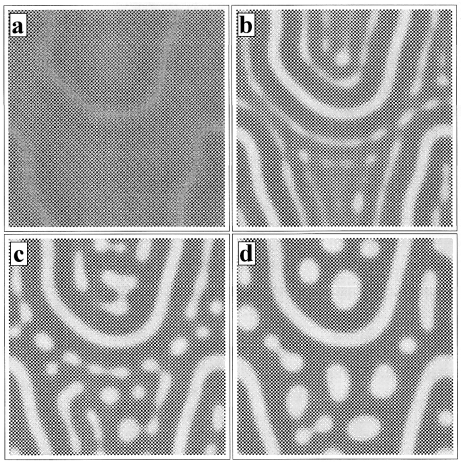

FIG. 9. Same as in Fig. 7, but at $c=0.3$ and following t': (a) 0, (b) 500, (c) 1000, and (d) 2000.

Later on the usual coarsening process starts, by splitting or fusion of some of the stripes and evaporation of smaller precipitates; see Figs. 7(c)–7(f).

Figure 9 shows that this phenomenon is rather sensitive to the value of the composition c. When the difference in proportions of different phases in the mixture, $x_{\mathrm{ord}}-x_{\mathrm{disord}}\simeq 4c-1$, becomes important, the breaking of disordered layers with the formation of droplets starts competing with the replication mechanism, and replicated structures do not develop.

When looking for experimental manifestations of APB replication, we should keep in mind that homogeneous SD induced by thermal fluctuations in local occupations n_i is competing with replication. Such fluctuations are neglected in the MFA, in particular, in the MFKE where only ''averaged over distribution'' quantities $c_i=\langle n_i\rangle$ are considered;[10] however, these fluctuations are present in reality. The contribution of fluctuations to the patterning in the SD regime should be particularly important near the conditional or ordering spinodal, where the amplification of the above-discussed unstable concentration waves is slow. Therefore, in the c,T states close to spinodals, the APB replication under SD should be less pronounced.

Unfortunately, previous structural studies of SD under ordering known to us[1,2] seem to be performed just in the vicinity of the conditional spinodal. These studies do not reveal any distinct APB replication. However, Oki *et al.*[2] mentioned that ''some of the disordered phase appears in a layer along APB,'' while in the upper right part of Fig. 5(c) in Ref. 1 one can see a family of broken layers of the disordered phase that are approximately parallel to the adjacent APB.

In order to simulate the contribution of thermal fluctuations to the formation of embryos, we introduced in our simulation additional random fluctuations δc_{fi} just after annealing (i.e., at $t'=0$). For simplicity we supposed δc_{fi} to be random (just as the fluctuations δc_i introduced before annealing), while the actual embryo-creating fluctuations near spinodals seem to have considerable correlation lengths.[23] In our simulations, a significant competition between homogeneous SD and replication at APB's occurs only at relatively large fluctuation amplitudes $|\delta c_{fi}|\gtrsim 0.05$–$0.1$. However, these amplitudes can be made much smaller if we allow for space correlations of the fluctuations.

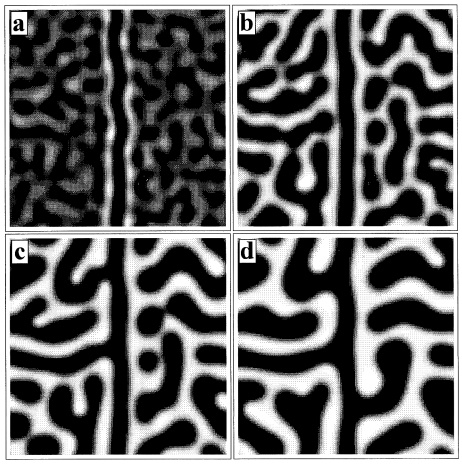

FIG. 10. Same as in Fig. 7 with the following modification: After the second quench ($T'=0.424$) random fluctuations δ_{fi} are introduced near the straight APB (see text); the pictures correspond to following t' values: (a) 100, (b) 500, (c) 1000, and (d) 2000. The completely dark area corresponds to the minimum concentration $\overline{c(\mathbf{R})}$ and to most disordered regions; the completely white, to the maximum $\overline{c(\mathbf{R})}$ and to most ordered regions; in between, $\overline{c(\mathbf{R})}$ varies linearly with darkness.

In Fig. 10 we present the results of simulations for the same model and parameter values as in Fig. 7, but introducing at $t'=0$ the above-described random fluctuations $\delta c_{fi}=\pm 0.1$ near a straight APB. In order to facilitate the comparison with the dark-field micrographs presented in Refs. 1 and 2, in Fig. 10 we invert the color code used up to now in the present paper: the most disordered area is completely dark, while the most ordered one is completely white. The simulated microstructures reveal a striking similarity with the observed ones.[1,2] Note, in particular, the presence of an ordered layer adjacent to APB's (the above-mentioned c bank) in Fig. 10, which is also distinctly seen in micrographs 5(b) and 5(c) in Ref. 1, or Fig. 1(b) and 1(c) (middle column) in Fig. 2. Later on in our simulation, dark ''branches'' of the disordered phase begin to grow from APB's almost normal to it [Figs. 10(c) and 10(d)], which corresponds to the coagulation of nearby disordered precipitates with the APB. Such morphologies are also clearly seen experimentally, e.g., Figs. 1(c) and 1(d) (middle column) in Ref. 2. We repeated the above-described simulation with lower fluctuation amplitudes $\delta c_{fi}=\pm 0.04$, and obtained microstructures with broken layers of the disordered phase near the APB, similar to those in the upper right part of the micrograph 5(c) in Ref. 1.

Further structural studies of APB evolution under SD with ordering, in particular, for c,T values as far from spinodals as possible, can reveal clearer manifestations of the APB replication phenomenon.

V. APPLICATION OF THE MFKE TO A DESCRIPTION OF TRANSIENT ORDERED STATES UNDER DECOMPOSITION INTO DISORDERED PHASES

The possible formation of transient ordered phases under SDDA was considered by CK (Ref. 15) using the PLKE, and later on by Reinhardt and Turchi[16] (RT) using Monte Carlo (MC) simulations. The physical aspects and main features of

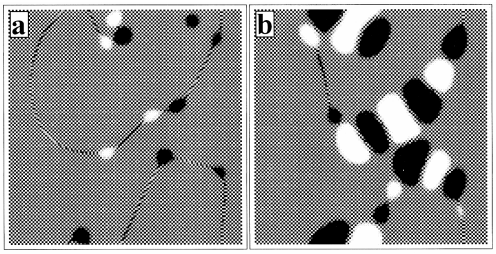

FIG. 11. Temporal evolution of the same 2D model as in Refs. 15 and 16 for a square lattice of 128×128 sites, at $c=0.5$, $T=\frac{1}{3}T_0$ and following t': (a) 400 and (b) 1900.

this phenomenon have been discussed by these authors. Below we address this problem with the aim of estimating the accuracy of the MFKE, taking MC simulation[16] as a reference for the same model.

Possible shortcomings of mean-field-type approaches in describing the transient ordered states kinetics have been discussed by RT.[16] They noted that the main qualitative features of evolution found by CK,[15] such as precipitation of the disordered phase on APB's, the presence of ordered interfaces between the disordered product phases, etc., have been confirmed by the MC simulations.[16] However, two differences have been found. (i) The ordering spinodal in the MF approach[15] delineates regions with distinctly different kinetic behavior, while MC simulations show a gradual change of evolution under variation of c and T, and (ii) MC simulations show a coexistence near APB's of three phases, A-rich disordered, B-rich disordered, and ordered phases, while CK (Ref. 15) did not observe such microstructures. RT ascribed the differences to inherent limitations of the MFA.

Discrepancy (i) is analogous to that for spinodals in usual SDDA where MC simulations do not show sharp changes in kinetic behavior when the c,T point crosses the spinodal curve,[20] while in the MFA this curve limits the infinitesimal fluctuation instability area. The discrepancy is usually believed to be due to inaccuracies in the MFA.[20] However, experiments[2] mentioned in Sec. I appear to show that the borderline in the c,T plane between areas of the different decomposition kinetics is rather sharp, indeed. Therefore, at least for the FeAl alloys studied in Ref. 2, the spinodal curve (in this case, the conditional spinodal) can apparently be defined with a sufficient accuracy.

To clarify the origin of discrepancy (ii), we made simulations based on the MFKE for the same model and parameter values as those in Ref. 16: $c=0.5$, $T=\frac{1}{3}T_0$ where T_0 is the critical temperature for SDDA. In our results the discrepancy (ii) is absent. For example, Fig. 11 shows both creation of disordered islands along APB's and coexistence at intermediate times of three phases, ordered, gaslike, and liquidlike, with the ordered interfaces between the latter two phases. The morphologies shown in Figs. 11(a) and 11(b) are rather similar to those in Figs. 4(b) and 4(c) in Ref. 16 and look like their ''averaged over thermal fluctuations'' versions, in accordance with the averaged character of the MFKE and a sufficiently large interaction range in the model[15] used.

Therefore, the discrepancy (ii) is not inherent to the MFA as RT supposed, but can be connected either with the difference in compositions ($c=0.175$ or 0.25 in Ref. 15, while $c=0.5$ in Ref. 16), or with possible shortcomings of the PLKE used in Ref. 15.

VI. CONCLUSIONS

This work investigates the decomposition kinetics under alloy ordering with the use of the earlier derived mean-field kinetic equation.[10] To describe the first stage of decomposition, we present the linear stability analysis for small fluctuations in local concentration and order parameter in the homogeneous ordered alloy. The analysis generalizes that given by Cahn[7] for the disordered alloys; it provides explicit expressions for increments p of fluctuation waves, as well as for the maximum value $p_{\max}=p_c$ and for the corresponding wave number $k=k_c$ that correspond to the fastest growing, critical waves. The strong interaction between the concentration and the order parameter results in a number of differences in the functional form $p(\mathbf{k},c,T)$, $p_c(c,T)$, and $k_c(c,T)$ as compared to disordered alloys. In particular, when the initial c,T point is close to the ordering spinodal, critical fluctuations grow with time much faster than in the disordered alloys with the same distance ζ to the spinodal, while near the conditional spinodal defined in Ref. 1, the dependences $p(\mathbf{k},\zeta)$, $p_c(\zeta)$, and $k_c(\zeta)$ are similar to those for the disordered alloy.

We also studied the microstructural evolution under decomposition with ordering for various types of quenches to the two-phase equilibrium region. Our results illustrate and specify general considerations of Allen and Cahn[1] about the variability and features of this evolution. We found, in particular, that for the single-domain ordered initial state, the evolution under such SD is generally similar to that for disordered alloys. However, when the initial AP domain size is of the order of the characteristic critical length $\lambda_c=2\pi/k_c$, transient microstructures under SD become sensitive to the initial composition c. In particular, at large $c\gtrsim c_t$ where c_t is the composition at the tricritical point, the initial AP domain structure is basically preserved at large time, and morphologies for these later times are determined by the initial structure. We also considered the quench (a)$\rightarrow$(e) into the metastable area (e) in Fig. 1 and studied the features of the evolution from the initial APB-shaped precipitate to the final single-connected one.

A peculiar phenomenon of APB replication, i.e., the formation of quasiperiodic structures replicating the form of the initial APB form, can arise near isolated APB's under SD with ordering. We discuss possible experimental evidence thereof: Some available experimental data [1,2] seem to support the theoretical findings.

Finally, we compare the description of transient ordered states under SD given by our MFKE with that obtained in a Monte Carlo study.[16] We find that the two descriptions are in good qualitative agreement. This seems to confirm the applicability of the MFKE to studies of phenomena treated in the present work.

ACKNOWLEDGMENTS

This work was supported by the International Science Foundation under Grant No. MQA300 and by the Russian Fund of Fundamental Research under Grant No. 95-02-06426.

[1] S. M. Allen and J. W. Cahn, Acta Metall. **24**, 425 (1976).
[2] K. Oki, H. Sagane, and T. Eguchi, J. Phys. (Paris) Colloq. **38**, C7-414 (1977).
[3] L. Q. Chen and A. G. Khachaturyan, Acta Metall. Mater. **39**, 2533 (1991).
[4] L. Q. Chen, Y. Z. Wang, and A. G. Khachaturyan, in *Statics and Dynamics of Alloy Phase Transformations*, Vol. 319 of *NATO Advanced Study Institute, Series B: Physics*, edited by A. Gonis and P. E. A. Turchi (Plenum, New York, 1994), pp. 587–604.
[5] L. Q. Chen, Mod. Phys. Lett. **7**, 1857 (1993).
[6] L. D. Landau and E. M. Lifshitz, *Statistical Physics* (Nauka, Moscow, 1976), Pt. 1.
[7] J. W. Cahn, Acta Metall. **9**, 795 (1961).
[8] J. W. Cahn and R. Kikuchi, J. Phys. Chem. Solids **27**, 1305 (1966).
[9] V. Yu. Dobretsov, G. Martin, F. Soisson, and V. G. Vaks, Europhys. Lett. **31**, 417 (1995).
[10] V. G. Vaks, S. V. Beiden, and V. Yu. Dobretsov, Pis'ma Zh. Éksp. Teor. Fiz. **61**, 65 (1995) [JETP Lett. **61**, 68 (1995)].
[11] G. Martin, Phys. Rev. B **50**, 12 362 (1994).
[12] V. G. Vaks and S. V. Beiden, Zh. Éksp. Teor. Fiz. **105**, 1017 (1994) [Sov. Phys. JETP **78**, 546 (1994)].
[13] V. G. Vaks, A. I. Larkin, and S. A. Pikin, Zh. Éksp. Teor. Fiz. **51**, 361 (1966) [Sov. Phys. JETP **24**, 240 (1967)].
[14] I. M. Lifshits and V. V. Slyozov, J. Phys. Chem. Solids **19**, 35 (1961).
[15] L. Q. Chen and A. G. Khachaturyan, Phys. Rev. B **44**, 4681 (1991).
[16] L. Reinhard and P. E. A. Turchi, Phys. Rev. Lett. **72**, 120 (1994).
[17] G. Martin, Phys. Rev. B **41** 2279 (1990).
[18] S. V. Beiden, V. Yu. Dobretsov, G. Martin, F. Soisson, and V. G. Vaks, in *Stability of Materials*, *NATO Advanced Study Institute*, edited by A. Gonis, P. E. A. Turchi, and J. Kudrnovsky (Plenum Press, New York, in press).
[19] K. Gschwend, H. Sato, and R. Kikuchi, J. Chem. Phys. **69**, 5006 (1978).
[20] J. D. Gunton, M. San Miguel, and P. Sahni, in *Phase Transitions and Critical Phenomena*, edited by C. Domb and J. H. Lebowitz (Academic, London, 1983), Vol. 8, pp. 269–466.
[21] Y. Oono and S. Puri, Phys. Rev. Lett. **58**, 836 (1987).
[22] G. Martin and F. Soisson F, J. Phys. (France) IV Colloq. **5**, C3-317 (1995).
[23] J. W. Cahn and J. E. Hilliard, J. Chem. Phys. **31**, 688 (1959).